



Ultrathin bismuth oxyiodide nanosheets for photocatalytic ammonia generation from nitrogen and water under visible to near-infrared light

M. Mohebinia ^a, C. Wu ^{b,c}, G. Yang ^a, S. Dai ^{c,d}, A. Hakimian ^e, T. Tong ^c, H. Ghasemi ^e, Z. Wang ^b, D. Wang ^f, Z. Ren ^f, J. Bao ^{a,c,f,*}

^a Material Science and Engineering, University of Houston, Houston, TX, 77204, USA

^b Institute of Fundamental and Frontier Sciences, University of Electronic Science and Technology of China, Chengdu, Sichuan, 610054, China

^c Department of Electrical and Computer Engineering, University of Houston, Houston, TX, 77204, USA

^d College of Electronics and Information Engineering, Sichuan University, Chengdu, Sichuan, 610065, China

^e Department of Mechanical Engineering, University of Houston, Houston, TX, 77204, USA

^f Department of Physics and Texas Center for Superconductivity, University of Houston, Houston, TX, 77204, USA



ARTICLE INFO

Article history:

Received 22 July 2020

Received in revised form

9 September 2020

Accepted 16 September 2020

Available online 19 September 2020

Keywords:

BiOI

Photocatalysis

N₂ fixation

Band edge position

Surface dipole

ABSTRACT

Artificial photosynthesis of ammonia using atmospheric nitrogen and water is a sustainable but challenging alternative to the Haber-Bosch process. Bismuth oxyiodide (BiOI) is a promising candidate due to its superior light absorption capability (bandgap of around 1.8 eV) and abundant surface oxygen vacancies. However, its improper band edge positions made it inactive for overall water-splitting and N₂ fixation. In this work, ultrathin BiOI nanosheets were synthesized through a simple surfactant (PVP) assisted hydrothermal route. The nanosheets split pure water into H₂ and O₂ and converted nitrogen and water into ammonia under visible or near-infrared light. PVP capping not only reduced the thickness of BiOI sheets but also upshifted its band edge positions due to the surface electric dipole induced by polyvinyl pyrrolidone molecules on the BiOI surface, thus enabling the water oxidation and nitrogen reduction half reactions simultaneously.

© 2020 Elsevier Ltd. All rights reserved.

1. Introduction

Nitrogen fixation in nature using nitrogenase is an astonishing catalytic reaction for millions of years [1]. Artificial photosynthesis of ammonia using photocatalysts as a green and sustainable process has also attracted enormous attention [2]. For this purpose, many photocatalysts have been reported to reduce nitrogen to ammonia; however, they are either wide bandgap semiconductors that absorb ultraviolet light or have to use hole scavenger sacrificial reagents [3–6]. For example, Bi₂O₃ and BiO can reduce N₂ without any organic sacrificial reagent under UV light (<435 nm, and <430 nm, respectively) [6,7], while graphitic carbon nitride (g-C₃N₄) is active under visible light, but requires sacrificial reagents [8,9]. The development of single photocatalysts that can generate ammonia from N₂ and pure water utilizing visible and even near-

infrared light turns out to be challenging [10]. It was not until last year Zhao et al. showed that doping TiO₂ with copper can make it active even under near-infrared light [11]. Compared to photocatalytic solar water splitting, there are more material requirements for N₂ fixation [2]. First, N₂ reduction is a multi-electron charge transfer process as opposed to a single electron in the hydrogen evolution reaction (HER) [12,13]. Second, depending on different reaction routes, N₂ fixation typically requires a higher reduction potential than HER [13], so many of water splitting photocatalysts are not active for N₂ fixation [14].

In this work, we report a new photocatalyst that can generate ammonia from N₂ and water without any sacrificial reagents under illumination from visible to near-infrared light. Ultrathin BiOI nanosheets were prepared via a surfactant assisted hydrothermal method. Unlike the macroscopic sheets, BiOI nanosheets are also active for overall photocatalytic water splitting. Our bandgap and band edge position characterizations by UV–Vis, photoluminescence, Mott–Schottky, and Kelvin probe revealed that the activity of BiOI nanosheets originates from their upshifted band

* Corresponding author.

E-mail addresses: jbao@central.uh.edu, jbao@uh.edu (J. Bao).

edge positions, which makes its band edges aligned perfectly with water splitting and N₂ reduction potentials. Furthermore, abundant native oxygen vacancies provide more active sites for adsorption and activation of nitrogen molecules on BiOI-NS surfaces.

2. Results and discussion

Ultrathin nanosheets (denoted as BiOI-NS) were synthesized by a surfactant (PVP) assisted hydrothermal method [15]. 1 mmol Bi(NO₃)₃·5H₂O was first dissolved in a mixture of 30 mL ethylene glycol and 5 mL deionized water (DI) water, followed by adding a stoichiometric amount of KI to yield an orange solution. Subsequently, 200 mg polyvinyl pyrrolidone was added into the solution, and the resulting orange suspension was stirred vigorously for 1 h. The final solution was poured in a 40 mL teflon autoclave and placed in oven at 160 °C for 8 h. The resulting powder was washed and dried afterward. Powder X-ray diffraction was first used to examine the crystal structure of the resulting BiOI powder. The characteristic peaks at (110) and (102) in Fig. 1a confirm its layered tetragonal crystal structure despite differing in line width and intensity. In fact, these unique XRD patterns revealed the ultrathin nature of 2D BiOI nanosheets. The sharp line at (110) indicates a high crystal quality in the basal plane with an average size of 21.4 nm based on the Scherrer equation. The weak and broad out-

of-plane peaks reflect extremely thin sheets of 2D structure. The missing (002) peak indicates that the thickness is beyond XRD detection. Based on the (102) peak, the thickness is limited to 3.5 nm, which is also confirmed by the atomic force microscopy image and height profile in Fig. S3. Transmission electron microscopy (TEM) image confirmed the shape and size of the ultrathin nanosheets. Low resolution TEM images in Fig. 1b shows that the lateral size of nanosheets is around 30–50 nm, high resolution TEM in Fig. 1c confirmed that NS are only a few layers thick, lattice fringe images in Fig. 1d and e suggest a high crystal quality of NS [16].

Photocatalytic N₂ fixation tests were carried out by continuously flowing N₂ into the aqueous suspension of BiOI-NS without sacrificial reagent. The concentration of ammonia in the solution was determined with the indophenol blue method [17,18] and was monitored each hour by taking out 2 mL of the solution. Under the white light irradiation from a xenon lamp, Fig. 2a shows that NH₃ concentration in the solution increased linearly with time. Control experiments confirmed that the reaction was photocatalytic because blocking the light or replacing N₂ with Ar totally suppressed the production of NH₃ (Fig. 2a). Additionally, the BiOI-NS sample showed good stability under the light illumination after five cycles (Fig. 2b).

Because PVP contains nitrogen in its structure, it can interfere with ammonia generation and detection. To further confirm the photocatalytic reaction, we performed isotope labeling experiments using pure ¹⁵N₂ and nuclear magnetic resonance (NMR) (Fig. S4). Proton NMR is a very sensitive method as it can distinguish ¹⁵N from ¹⁴N nuclei in the form of ammonium ion [19,20]. Fig. 2c shows the proton NMR results after using ¹⁴N₂ and ¹⁵N₂ gases as precursors for the nitrogen reduction reaction. The emergence of two characteristic peaks of ¹⁵NH₄⁺ from the initial three peaks of ¹⁴NH₄⁺ ions after using ¹⁵N₂ gas confirmed that N₂ was the source for photocatalytic ammonia generation [20,21].

Bismuth oxyhalides BiOXs (X = Cl, Br, and I) have been extensively used as photocatalysts for applications in pollutant removal, dye degradation and water splitting [22–25]. However, only in 2015, BiOBr was first reported to perform photocatalytic N₂ fixation under visible light [14]. Soon after that, BiOXs attracted lots of attention due to their controllable bandgaps (3.2–1.8 eV) and energetic surface sites for nitrogen activation [4,5,14]. Among them, BiOI is very well-suited for solar light harvesting thanks to its small bandgap of around 1.8 eV [26,27]. But in one work, BiOI was reported to do photocatalytic N₂ fixation with an organic sacrificial reagent [28]; in another work, BiOI was used for photoelectrochemical oxygen evolution (OER), in other words, it was only active for OER, and it could not evolve hydrogen under light illumination [29].

To resolve this discrepancy and understand the origin of the activity of our BiOI-NS, we synthesized two more BiOI samples (both labeled as pristine BiOI) using either water or ethylene glycol as a solvent and compared their activity with that of BiOI-NS. Fig. S1 shows their XRD and SEM, indicating their high crystal quality. It is shown that the diameter of the both pristine BiOI samples were around 4 μm, however, the thickness of the BiOI slabs along [002] was determined to be 50 nm for the sample prepared in water as solvent, and 20 nm for the sample prepared in ethylene glycol as the solvent. The photocatalytic experiments were performed at the same conditions. Fig. S6 shows that no ammonia was generated, so pristine BiOI is not active for N₂ fixation.

To further confirm their huge difference in N₂ fixation between BiOI-NS and pristine BiOI, we compared their activity for photocatalytic overall water splitting. It was quickly found that without Pt co-catalyst, both BiOI-NS and pristine BiOI are not active for overall water splitting. However, when decorated with Pt co-catalyst, BiOI-NS was able to split pure water into H₂ and O₂,

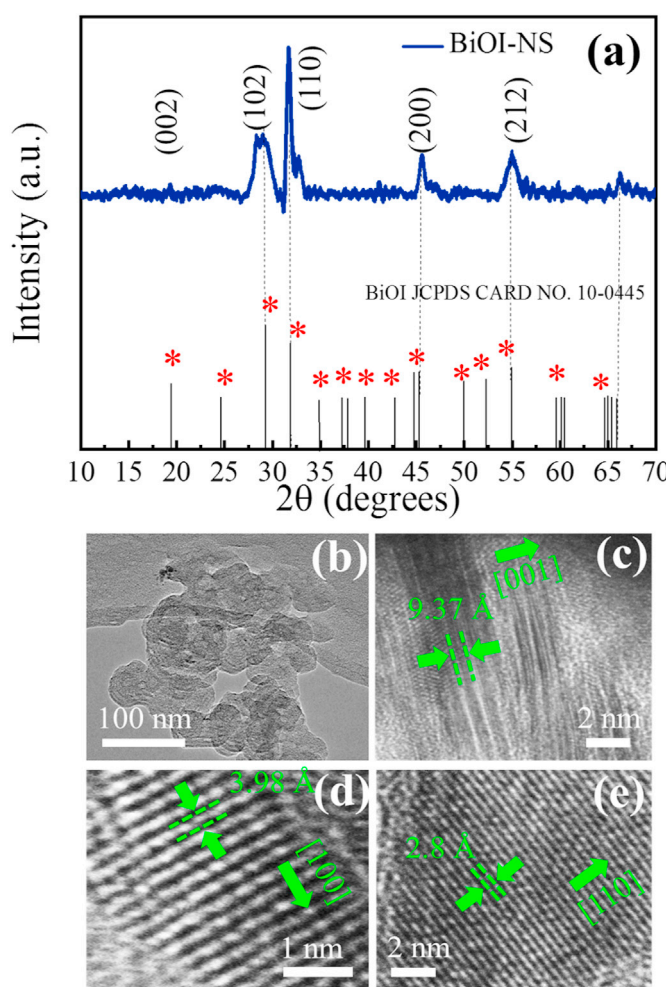


Fig. 1. BiOI nanosheet structure characterizations. (a) XRD diffraction pattern of BiOI nanosheets. (b) Low resolution and (c–e) high resolution TEM images of ultrathin BiOI nanosheets.

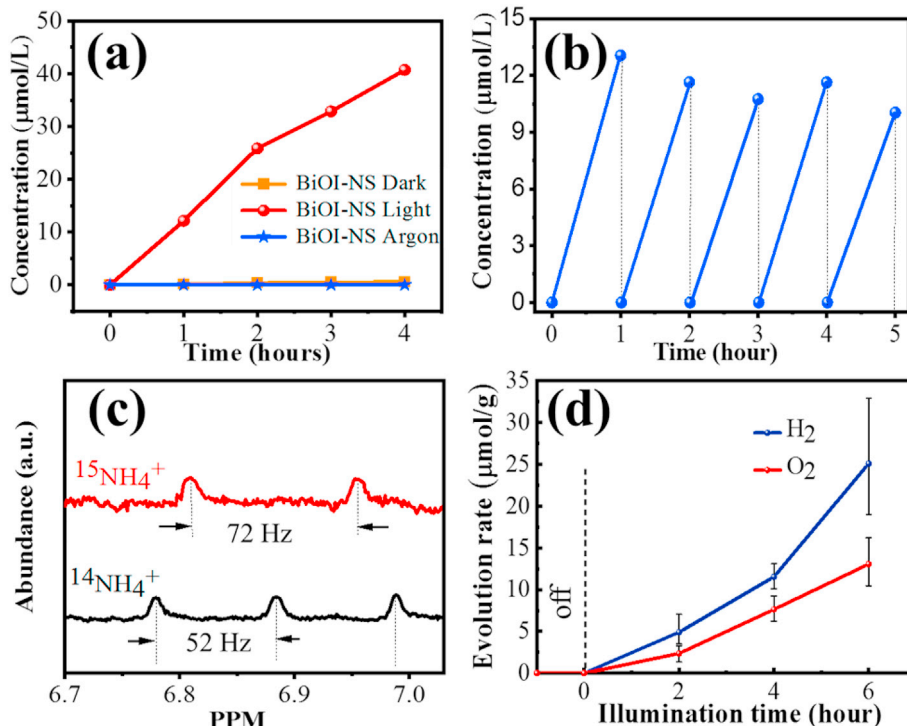


Fig. 2. Photocatalytic nitrogen fixation. (a) Ammonia generation in (red) nitrogen and (blue) argon saturated water under light, in (orange) nitrogen saturated water in the dark. (b) Cyclic stability of the nanosheets after 5 photocatalytic test cycles. (c) Proton NMR results for pure $^{15}\text{N}_2$ gas and $^{14}\text{N}_2$ gas fixation under the light illumination on BiOI-NS sample. (d) Overall water splitting. (For interpretation of the references to colour in this figure legend, the reader is referred to the Web version of this article.)

while pristine BiOI still remained inactive. Fig. 2d shows that the molar ratio of the hydrogen to oxygen is close to the ideal value of 2:1.

The different activities of BiOI for water splitting point to us that they may have different bandgaps and band edge positions, which are essential to the activity of any photocatalyst for both water splitting and N_2 fixation. As a first step, we compared their bandgaps because the change in bandgap will also result in the change in band edge positions. Fig. 3a and b shows UV-visible diffuse reflectance and the associated Tauc plot. It can be seen that they have a similar bandgap around 1.85 eV, very close to the reported values [16,30,31]. A slightly higher bandgap of BiOI-NS is due to its thinner sheets and the quantum confinement effect [27,32]. This small blueshift of absorbance is also confirmed with photoluminescence spectra in Fig. 3c. However, the photoluminescence as well as photoconductivity in Fig. 3d reveals a significant difference between BiOI-NS and pristine BiOI. BiOI-NS exhibits a much enhanced PL and photoconductivity, indicating a high crystal quality and longer lifetime of photo-excited electrons and holes [33,34], consistent with XRD and TEM evaluation.

The slightly higher bandgap and better crystal quality are certainly not enough to account for the activity of BiOI-NS, so we continue to employ two other techniques: Mott-Schottky and Kelvin probe to determine their Fermi levels (flat band potentials) and band edge positions [35,36]. As expected, Mott-Schottky plots in Fig. 4a reveals a big difference in their flat band potentials; while both BiOI-NS and pristine BiOI show positive slopes, indicating n-type semiconductors due to native oxygen vacancies [37,38]. The lower positive slope of BiOI-NS indicates that BiOI-NS has a higher concentration of oxygen vacancies, which is also confirmed by electron paramagnetic resonance (EPR) in Fig. 4b [39]. The negative shift of flat band potential of BiOI-NS to -0.12 V is significant as this will enable BiOI-NS to do HER and N_2 fixation. This negative shift of

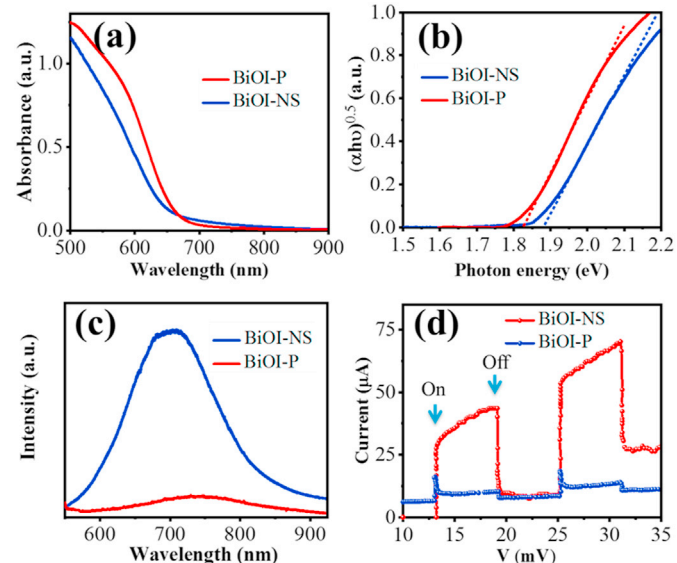


Fig. 3. Optical properties of BiOI crystals. (a) Optical absorbance of pristine and ultrathin nanosheets. (b) Optical band gap of BiOI-P, and BiOI-NS. (c) The photoluminescence spectra of different BiOI samples. (d) Photoconductivity of the BiOI-NS compared to pristine sample. “On” and “Off” indicate the on and off of light, respectively.

flat band potential or the upshift of the Fermi level is confirmed by the Kelvin probe in Fig. 4c. Considering the conduction band edge position (V_c) is ~ 0.3 eV above the Fermi level for an n-type semiconductor [7,40], its approximate band edge positions vs. H_2O and N_2 redox potentials in Fig. 4d explain why BiOI-NS become suitable for both nitrogen fixation and water splitting.

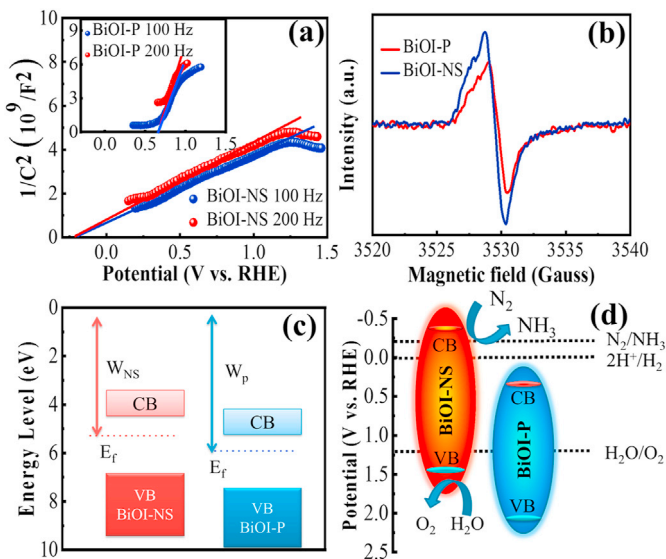


Fig. 4. Band edge positions. (a) Mott-Schottky plots of BiOI-P and BiOI-NS samples. (b) Electron paramagnetic resonance (EPR) spectra of BiOI-NS and BiOI-P in dark and at room temperature. (c) Work function of pristine BiOI and ultrathin nanosheets from vacuum level 0 V. (d) Schematic of band edge energies of BiOI ultrathin nanosheets vs. the standard reduction potentials of redox species for water splitting and nitrogen fixation at pH = 0 [3].

It is very well known that the surface dipole layer can change the work function or band edge positions [41–43]. The electric fields induced by the microscopic surface dipole layer can hinder or facilitate further charge transfer to the vacuum, in other words, it can change the work function [41]. PVP molecules, as widely reported before, can be attached to the surface of a material by the oxygen atoms at their pyrrolidone rings [44–46], resulting in an outward pointing surface electric dipole [47–49]. Such dipoles have been reported to significantly reduce the work function of silver nanorods [50]. The PVP oxygen bonding to BiOI can be confirmed by monitoring the change of C=O stretching mode at 1658 cm⁻¹.

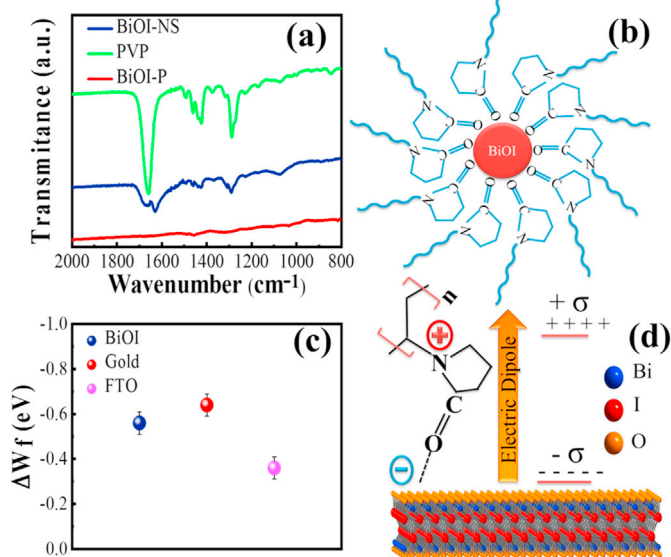


Fig. 5. BiOI functionalization by PVP. (a) FTIR spectra of BiOI-NS, BiOI-P and pure PVP. (b) Schematic of BiOI functionalization by PVP. (c) Work function change as a result of PVP coating. (d) Schematic of surface dipole moment induced by PVP.

FTIR spectra in Fig. 5a show that after PVP functionalization of BiOI-NS, a red-shifted peak at 1625 cm⁻¹ appears as expected. The same red shift was also reported when PVP was attached to the surface of gold particles [51,52]. Therefore, the reduction in work function by PVP functionalization is general and can be applied to other materials such as gold and FTO in addition to BiOI, as shown in Fig. 5c [53]. Fig. 5b and d illustrate the attached PVP molecules and the associated dipoles on BiOI surfaces, which are responsible for the reduction of their work function compared to the PVP free BiOI-P.

Photocatalytic N₂ fixation under visible light still remains a challenge, and here we further demonstrate that BiOI-NS is active under visible to near infrared light. For this purpose, the ammonia generation rate was measured with monochromatic light. Under 633 nm and 660 nm lights (100 mW/cm²), the ammonia generation rate was measured to be 1.15 μmol g⁻¹ h⁻¹ and 0.8 μmol g⁻¹ h⁻¹, respectively. BiOI even exhibits photocatalytic activity under illumination of 700 nm light, making it near-infrared active although with a reduced efficiency (Fig. S7). Note that these efficiencies are under estimated because the scattered light was not considered. Previously, N₂ fixation under near-infrared light was achieved in copper doped TiO₂, but still its intrinsic bandgap is in the UV range [11]. N₂ fixation under longer wavelength (800 nm) light was also demonstrated using hot electrons from plasmonic gold nanorods, but it requires a sacrificial reagent [20,54].

3. Conclusion

In conclusion, we demonstrated a narrow band gap photocatalyst that can perform N₂ fixation under visible to near-infrared light without any sacrificial reagents. The activity of BiOI nanosheets is enabled by PVP surface modification which not only reduces the thickness of BiOI nanosheets, but also upshifts its band edge position. The surface engineering of narrow band gap semiconductors provides a new approach to the development of highly efficient photocatalysts for ammonia generation from water and nitrogen using renewable solar energy.

Declaration of competing interest

The authors declare that they have no known competing financial interests or personal relationships that could have appeared to influence the work reported in this paper.

Acknowledgement

The authors gratefully acknowledge support from Welch Foundation (E-1728).

Appendix A. Supplementary data

Supplementary data to this article can be found online at <https://doi.org/10.1016/j.mtphys.2020.100293>.

References

- [1] D.E. Canfield, A.N. Glazer, P.G. Falkowski, The evolution and future of Earth's nitrogen cycle, *Science* 330 (2010) 192–196.
- [2] X. Chen, N. Li, Z. Kong, W.-J. Ong, X. Zhao, Photocatalytic fixation of nitrogen to ammonia: state-of-the-art advancements and future prospects, *Mater. Horizons* 5 (2018) 9–27.
- [3] Y. Shiraishi, M. Hashimoto, K. Chishiro, K. Moriyama, S. Tanaka, T. Hirai, Photocatalytic dinitrogen fixation with water on bismuth oxychloride in Chloride solutions for solar-to-chemical energy conversion, *J. Am. Chem. Soc.* 142 (2020) 7574–7583.
- [4] H. Li, J. Shang, J. Shi, K. Zhao, L. Zhang, Facet-dependent solar ammonia synthesis of BiOCl nanosheets via a proton-assisted electron transfer pathway, *Nanoscale* 8 (2016) 1986–1993.
- [5] Y. Bai, L. Ye, T. Chen, L. Wang, X. Shi, X. Zhang, D. Chen, Facet-dependent

- photocatalytic N₂ fixation of bismuth-rich Bi₅O₇I nanosheets**, *ACS Appl. Mater. Interfaces* 8 (2016) 27661–27668.
- [6] B. Liu, N. Wu, **Visible-light photocatalytic nitrogen fixation and electrons Transport in bismuth iron molybdate**, *ECS Meet. Abstr. MA2020–01* (2020) 2584.
- [7] X. Gao, Y. Shang, L. Liu, F. Fu, **Chemisorption-enhanced photocatalytic nitrogen fixation via 2D ultrathin p–n heterojunction AgCl/δ-Bi₂O₃ nanosheets**, *J. Catal.* 371 (2019) 71–80.
- [8] S. Sun, Q. An, W. Wang, L. Zhang, J. Liu, W.A. Goddard III, **Efficient photocatalytic reduction of dinitrogen to ammonia on bismuth monoxide quantum dots**, *J. Mater. Chem. A* 5 (2017) 201–209.
- [9] G. Dong, W. Ho, C. Wang, **Selective photocatalytic N₂ fixation dependent on gC₃N₄ induced by nitrogen vacancies**, *J. Mater. Chem. A* 3 (2015) 23435–23441.
- [10] J. Li, H. Li, G. Zhan, L. Zhang, **Solar water splitting and nitrogen fixation with layered bismuth oxyhalides**, *Acc. Chem. Res.* 50 (2017) 112–121.
- [11] Y. Zhao, Y. Zhao, R. Shi, B. Wang, G.I.N. Waterhouse, L. Wu, C. Tung, T. Zhang, **Tuning oxygen vacancies in ultrathin TiO₂ nanosheets to boost photocatalytic nitrogen fixation up to 700 nm**, *Adv. Mater.* 31 (2019) 1806482.
- [12] S. Zhang, Y. Zhao, R. Shi, G.I.N. Waterhouse, T. Zhang, **Photocatalytic ammonia synthesis: Recent progress and future**, *EnergyChem* 1 (2019) 100013.
- [13] X. Xue, R. Chen, C. Yan, P. Zhao, Y. Hu, W. Zhang, S. Yang, Z. Jin, **Review on photocatalytic and electrocatalytic artificial nitrogen fixation for ammonia synthesis at mild conditions: advances, challenges and perspectives**, *Nano Res* 12 (2019) 1–21.
- [14] H. Li, J. Shang, Z. Ai, L. Zhang, **Efficient visible light nitrogen fixation with BiOBr nanosheets of oxygen vacancies on the exposed {001} facets**, *J. Am. Chem. Soc.* 137 (2015) 6393–6399.
- [15] B. Li, L. Shao, B. Zhang, R. Wang, M. Zhu, X. Gu, **Understanding size-dependent properties of BiOCl nanosheets and exploring more catalysis**, *J. Colloid Interface Sci.* 505 (2017) 653–663.
- [16] P. Li, X. Zhao, C. Jia, H. Sun, L. Sun, X. Cheng, L. Liu, W. Fan, ZnWO₄/BiO heterostructures with highly efficient visible light photocatalytic activity: the case of interface lattice and energy level match, *J. Mater. Chem. A* 1 (2013) 3421–3429.
- [17] X. Gao, L. An, D. Qu, W. Jiang, Y. Chai, S. Sun, X. Liu, Z. Sun, **Enhanced photocatalytic N₂ fixation by promoting N₂ adsorption with a co-catalyst**, *Sci. Bull.* 64 (2019) 918–925.
- [18] L.F. Greenlee, J.N. Renner, S.L. Foster, **The use of controls for consistent and accurate measurements, of electrocatalytic ammonia synthesis from dinitrogen** 8 (2018) 7820–7827.
- [19] S.L. Deev, I.A. Khalymbadzha, T.S. Shestakova, V.N. Charushin, O.N. Chupakhin, ¹⁵N labeling and analysis of ¹³C–¹⁵N and ¹H–¹⁵N couplings in studies of the structures and chemical transformations of nitrogen heterocycles, *RSC Adv.* 9 (2019) 26856–26879.
- [20] C. Hu, X. Chen, J. Jin, Y. Han, S. Chen, H. Ju, J. Cai, Y. Qiu, C. Gao, C. Wang, **Surface plasmon enabling nitrogen fixation in pure water through a dissociative mechanism under mild conditions**, *J. Am. Chem. Soc.* 141 (2019) 7807–7814.
- [21] J. Liu, M.S. Kelley, W. Wu, A. Banerjee, A.P. Douvalis, J. Wu, Y. Zhang, G.C. Schatz, M.G. Kanatzidis, **Nitrogenase-mimic iron-containing chalcogels for photochemical reduction of dinitrogen to ammonia**, *Proc. Natl. Acad. Sci. Unit. States Am.* 113 (2016) 5530–5535.
- [22] S. Wang, L. Wang, W. Ma, D.M. Johnson, Y. Fang, M. Jia, Y. Huang, **Moderate valence band of bismuth oxyhalides (BiOXs; X= Cl, Br, I) for the best photocatalytic degradation efficiency of MC-LR**, *Chem. Eng. J.* 259 (2015) 410–416.
- [23] J. Hu, S. Weng, Z. Zheng, Z. Pei, M. Huang, P. Liu, **Solvents mediated-synthesis of BiOI photocatalysts with tunable morphologies and their visible-light driven photocatalytic performances in removing of arsenic from water**, *J. Hazard Mater.* 264 (2014) 293–302.
- [24] A.M. Alansari, M. Al-Qunaibit, I.O. Alade, T.F. Qahtan, T.A. Saleh, **Visible-light responsive BiOBr nanoparticles loaded on reduced graphene oxide for photocatalytic degradation of dye**, *J. Mol. Liq.* 253 (2018) 297–304.
- [25] L. Ye, Y. Su, X. Jin, H. Xie, C. Zhang, **Recent advances in BiOX (X= Cl, Br and I) photocatalysts: synthesis, modification, facet effects and mechanisms**, *Environ. Sci. Nano.* 1 (2014) 90–112.
- [26] H. Li, Z. Yang, J. Zhang, Y. Huang, H. Ji, Y. Tong, **Indium doped BiOI nanosheets: preparation, characterization and photocatalytic degradation activity**, *Appl. Surf. Sci.* 423 (2017) 1188–1197.
- [27] Z.-Y. Zhao, W.-W. Dai, **Electronic structure and optical properties of BiOI ultrathin films for photocatalytic water splitting**, *Inorg. Chem.* 54 (2015) 10732–10737.
- [28] L. Zeng, F. Zhe, Y. Wang, Q. Zhang, X. Zhao, X. Hu, Y. Wu, Y. He, **Preparation of interstitial carbon doped BiOI for enhanced performance in photocatalytic nitrogen fixation and methyl orange degradation**, *J. Colloid Interface Sci.* 539 (2019) 563–574.
- [29] L. Shan, L. He, J. Suriyaprakash, L. Yang, **Photoelectrochemical (PEC) water splitting of BiOI {001} nanosheets synthesized by a simple chemical transformation**, *J. Alloys Compd.* 665 (2016) 158–164.
- [30] T.B. Li, G. Chen, C. Zhou, Z.Y. Shen, R.C. Jin, J.X. Sun, **New photocatalyst BiOCl/BiOI composites with highly enhanced visible light photocatalytic performances**, *Dalton Trans.* 40 (2011) 6751–6758.
- [31] H. Lin, C. Zhou, J. Cao, S. Chen, **Ethylene glycol-assisted synthesis, photoelectrochemical and photocatalytic properties of BiOI microflowers**, *Chin. Sci. Bull.* 59 (2014) 3420–3426.
- [32] C. Wu, J. Zhang, X. Tong, P. Yu, J. Xu, J. Wu, Z.M. Wang, J. Lou, Y. Chueh, **A critical Review on enhancement of photocatalytic hydrogen production by Molybdenum Disulfide: from growth to interfacial activities**, *Small* 15 (2019) 1900578.
- [33] S. Yue, G.A. Gamage, M. Mohebinia, D. Mayerich, V. Talari, Y. Deng, F. Tian, S.-Y. Dai, H. Sun, V.G. Hadjiev, **Photoluminescence mapping and time-domain thermo-photooluminescence for rapid imaging and measurement of thermal conductivity of boron arsenide**, *Mater. Today Phys.* 13 (2020) 100194.
- [34] B. Giri, M. Masroor, T. Yan, K. Kushnir, A.D. Carl, C. Doiron, H. Zhang, Y. Zhao, A. McClelland, G.A. Tompsett, **Balancing light absorption and charge Transport in vertical SnS₂ Nanoflake Photoanodes with stepped layers and Large intrinsic mobility**, *Adv. Energy Mater.* 9 (2019) 1901236.
- [35] K. Gelderman, L. Lee, S.W. Donne, **Flat-band potential of a semiconductor: using the Mott–Schottky equation**, *J. Chem. Educ.* 84 (2007) 685–688.
- [36] D. Benetti, D. Cui, H. Zhao, F. Rosei, A. Vomiero, **Direct measurement of electronic band structure in single quantum dots of metal chalcogenide composites**, *Small* 14 (2018) 1801668.
- [37] N.T. Hahn, S. Hoang, J.L. Self, C.B. Mullins, **Spray pyrolysis deposition and photoelectrochemical properties of n-type BiOI nanoplatelet thin films**, *ACS Nano* 6 (2012) 7712–7722.
- [38] H. Wang, Y. Liang, L. Liu, J. Hu, P. Wu, W. Cui, **Enriched photoelectrocatalytic degradation and photoelectric performance of BiOI photoelectrode by coupling rGO**, *Appl. Catal. B Environ.* 208 (2017) 22–34.
- [39] S. Zhang, Y. Zhao, R. Shi, C. Zhou, G.I.N. Waterhouse, L. Wu, C. Tung, T. Zhang, **Efficient photocatalytic nitrogen fixation over Cu^{δ+}-modified defective ZnAl-layered Double Hydroxide nanosheets**, *Adv. Energy Mater.* 10 (2020) 1901973.
- [40] S. Bai, J. Jiang, Q. Zhang, Y. Xiong, **Steering charge kinetics in photocatalysis: intersection of materials syntheses, characterization techniques and theoretical simulations**, *Chem. Soc. Rev.* 44 (2015) 2893–2939.
- [41] L. Kronik, Y. Shapira, **Surface photovoltage phenomena: theory, experiment, and applications**, *Surf. Sci. Rep.* 37 (1999) 1–206.
- [42] T.C. Leung, C.L. Kao, W.S. Su, Y.J. Feng, C.T. Chan, **Relationship between surface dipole, work function and charge transfer: Some exceptions to an established rule**, *Phys. Rev. B* 68 (2003) 195408.
- [43] Y. Sun, Z. Liu, P. Pianetta, **Surface dipole formation and lowering of the work function by Cs adsorption on InP (100) surface**, *J. Vac. Sci. Technol. A Vacuum, Surfaces, Films*, 25 (2007) 1351–1356.
- [44] M. Behera, S. Ram, **Solubilization and stabilization of fullerene C₆₀ in presence of poly (vinyl pyrrolidone) molecules in water**, *J. Inclusion Phenom. Macrocycl. Chem.* 72 (2012) 233–239.
- [45] S. Ram, H.-J. Fecht, **Modulating up-energy transfer and violet-blue light emission in gold nanoparticles with surface adsorption of poly (vinyl pyrrolidone) molecules**, *J. Phys. Chem. C* 115 (2011) 7817–7828.
- [46] M. Behera, S. Ram, **Inquiring the mechanism of formation, encapsulation, and stabilization of gold nanoparticles by poly (vinyl pyrrolidone) molecules in 1-butanol**, *Appl. Nanosci.* 4 (2014) 247–254.
- [47] S. Haesuwannakij, T. Kimura, Y. Furutani, K. Okumura, K. Kokubo, T. Sakata, H. Yasuda, Y. Yakiyama, H. Sakurai, **The impact of the polymer chain length on the catalytic activity of poly (N-vinyl-2-pyrrolidone)-supported gold nanoclusters**, *Sci. Rep.* 7 (2017) 1–8.
- [48] H. Tsunoyama, N. Ichikuni, H. Sakurai, T. Tsukuda, **Effect of electronic structures of Au clusters stabilized by poly (N-vinyl-2-pyrrolidone) on aerobic oxidation catalysis**, *J. Am. Chem. Soc.* 131 (2009) 7086–7093.
- [49] M. Okumura, Y. Kitagawa, T. Kawakami, M. Haruta, **Theoretical investigation of the hetero-junction effect in PVP-stabilized Au13 clusters. The role of PVP in their catalytic activities**, *Chem. Phys. Lett.* 459 (2008) 133–136.
- [50] J. Li, Y. Tao, S. Chen, H. Li, P. Chen, M. Wei, H. Wang, K. Li, M. Mazzeo, Y. Duan, **A flexible plasma-treated silver-nanowire electrode for organic light-emitting devices**, *Sci. Rep.* 7 (2017) 1–9.
- [51] R.K. Gangwar, V.A. Dhumale, D. Kumari, U.T. Nakate, S.W. Gosavi, R.B. Sharma, S.N. Kale, S. Datar, **Conjugation of curcumin with PVP capped gold nanoparticles for improving bioavailability**, *Mater. Sci. Eng. C* 32 (2012) 2659–2663.
- [52] V.A. Dhumale, R.K. Gangwar, S.S. Datar, R.B. Sharma, **Reversible aggregation control of polyvinylpyrrolidone capped gold nanoparticles as a function of pH**, *Mater. Express.* 2 (2012) 311–318.
- [53] Y. Zhou, C. Fuentes-Hernandez, J. Shim, J. Meyer, A.J. Giordano, H. Li, P. Winget, T. Papadopoulos, H. Cheun, J. Kim, **A universal method to produce low-work function electrodes for organic electronics**, *Science* 336 (2012) 327–332.
- [54] H. Jia, A. Du, H. Zhang, J. Yang, R. Jiang, J. Wang, C. Zhang, **Site-selective growth of crystalline ceria with oxygen vacancies on gold nanocrystals for near-infrared nitrogen photofixation**, *J. Am. Chem. Soc.* 141 (2019) 5083–5086.